S23G-0448: Full waveform inversion reveals high-resolution crustal structure within the Southern Hikurangi Margin: Implications for physical conditions along the megathrust

Brook Tozer[1], Zeyu Zhao[2], Adrien Arnulf[3], Mrinal Sen[3], Susan Ellis[1] & Dan Bassett[1]

[1] GNS Science/Te Pu Ao, Avalon NZ
[2] Peking University, Bejing, China
[3] University of Texas Institute for Geophysics, USA

1) Rationale

- Recently, the first Full Waveform Inversion (FWI) derived images of the Hikurangi Subduction Zone have emerged from the northern and central sections of the margin [e.g. Arnulf et al., 2021 (05CM38); Bangs et al., 2023; Gase et al., 2023; (NZ3D Box); Fig. 1].
- These **high-fidelity depth-domain** images have revealed the structure of the upper ~ 7 km in unprecedented detail. Notably, **large velocity variations over short (10's km) length scales** are observed with **prominent low P-wave velocity (Vp) zones** within both the forearc and upper section of the subducting plate interpreted as regions of elevated fluid volume & pore-fluid pressure.
- Traditionally, **two major hurdles for performing FWI** have been:
  1. The **necessity of a well-constrained starting model** (usually derived by tomography prior to FWI).
  2. The **computational cost** of FWI as higher frequency content is included.
- In this study, we employ a new **FWI framework known as Hybrid FWI** [Zhao et al., 2022] which **effectively overcomes these limitations**, greatly relaxing the pre-processing burden and computational cost.
- Following the study of Arnulf et al., [2021], we repeat the analysis of profile 05CM38 to: (1) benchmark the new Hybrid FWI framework; (2) extend the imaging depth to ~ 9 km and (3) use the derived P-wave velocity field and tectonic structure to constrain numerical models of fluid release & effective pressure. We also present a preliminary FWI result from the southern margin along profile SAHKE01, where co-located OBS records are used to verify the derived V_p structure.

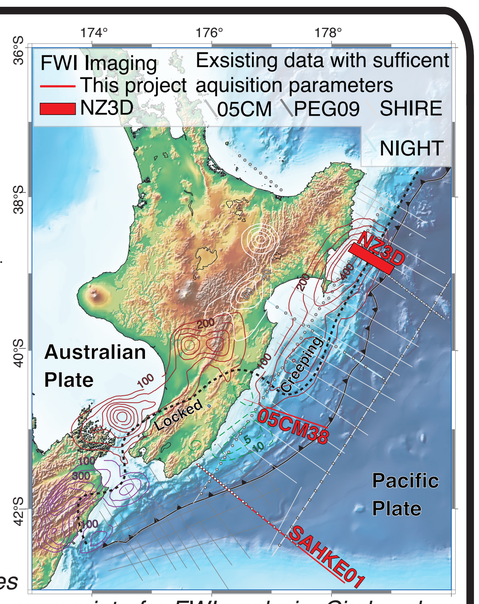

Fig 1: *Hikurangi Subduction Margin. Red lines show FWI profiles analysed in this study. Grey lines show exsisting 2D seismic surveys appropriate for FWI analysis. Circles show Ocean Bottom Seismometers. Coloured contours show slow-slip & after-slip patches, dashed black line shows locked/creeping sections (Wallace, 2022).*

2) Full Waveform Inversion Workflow

We apply the Hybrid FWI framework recently developed by **Zhao et al., (2022).** The workflow used to derive Fig. 3b was as follows:

Step 1- Shot gather pre-processing:
1. Downward-extratpolate to 75 m above the seafloor (effectively shifting the refracted arrival ahead of the seafloor reflection).
2. Optimal predictive deconvolution to minimise the bubble pulse effect.
3. 3-20 Hz bandpass filter.

Step 2 - Hybrid FWI inversion (global optimisation via VFSA):
- Three very simple starting models are used - all converge to similar result.
- Effectively avoid 'local minima' by exploring global model space.
- Outputs are averaged and used as input to local optimisation code.

Step 3 - Local optimisation - Using HFWI ouput as input.

Step 4 - Reverse Time Migration - Use v_p model to generate depth domain reflection section.

Fig 2: *Example SEAM salt model illustrating the utility of the Hybrid Optimisation method for recovering subsurface structure given a simple starting model [after Zhao et al., 2022]. a) Real subsurface Vp structure. b) Homogenous starting model. c) Recovered model using a traditional FWI approach. d) Recovered model after 3000 iterations using the hybrid FWI approach with global optimisation via Very Fast Simulated Annealing (VFSA). e) Final model generated using a local optimisation method and (d) as the starting model.*

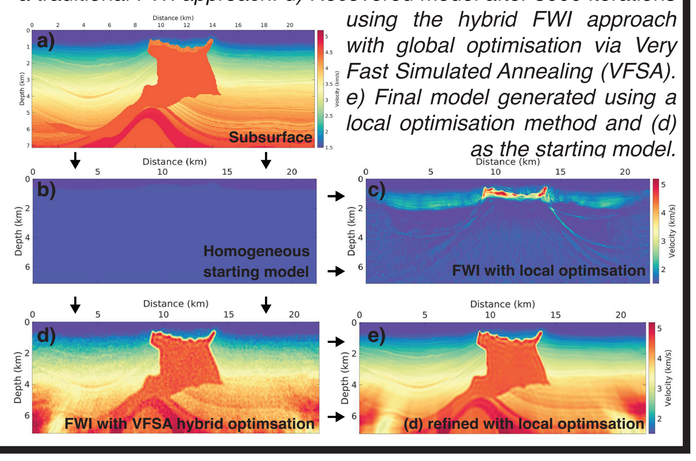

3) P-wave Velocity Models

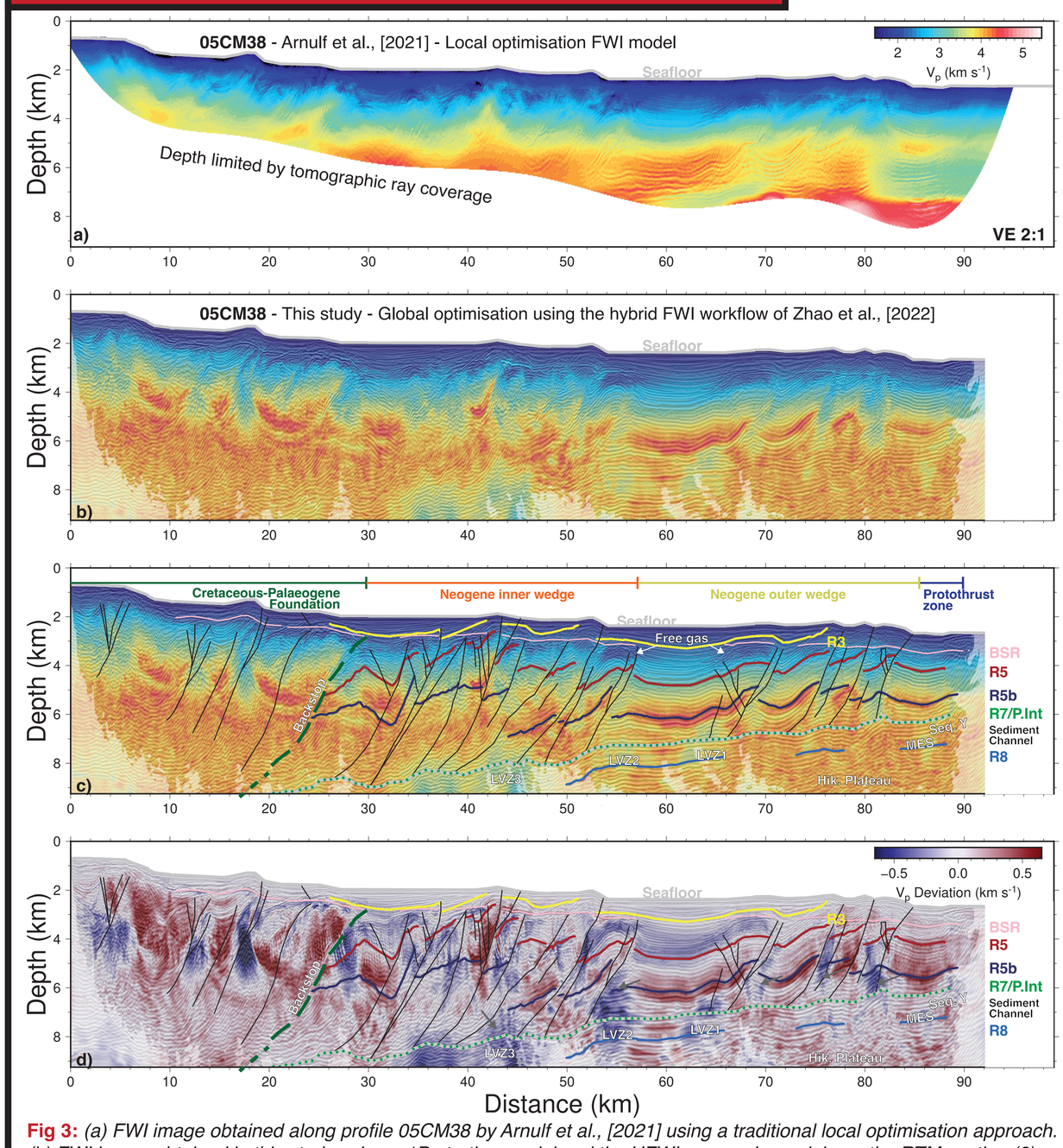

Fig 3: *(a) FWI image obtained along profile 05CM38 by Arnulf et al., [2021] using a traditional local optimisation approach. (b) FWI image obtained in this study using a 1D starting model and the HFWI approach overlain on the RTM section (2). Areas with relatively poor illumination are masked. (c) Interpretation following previous studies [Plaza-Faverola et al., 2016; Ghisetti et al., 2016; Arnulf et al., 2021]. Nomenclature follows Barnes et al., [2010]. black lines are major faults. LVZs = Low Velocity Zones in subducting sediment channel. (d) Deviation from sub-seafloor mean Vp highlighting lateral perturbations. Grey arrows highlight low velocity regions in the forearc, predominantly in thrust fault foot walls.*

Key findings:

- We successfully recover high-resolution V_p and depth domain reflection structure using a simple 1D starting model and extend imaging beyond that recovered in the Arnulf et al., [2021] study.
- Reductions in V_p are evident adjacent to major thrust faults. May reflect fluid pathways &/or higher porosity &/or fault damage zones.
- The plate interface reflection (R7) is tracked ~ 70 landward to a depth of ~ 9 km. This exhibits short wavelength roughness and a ~ 1 km deepening beneath the edge of the inner wedge coincident with the intersection of a major thrust fault.
- Low velocity Zones (LVZ) are imaged below the plate interface within the subducting Sequence-Y & MES sediment channel with a newly imaged prominent zone (LVZ3) beneath the inner wedge.

Key question:

What is the cause of the LVZs imaged within the subducting sediment channel? Hypothesis: Given their depth and the expected temperature structure, LVZs occur where we may expect H_20 release from mineral dehydration reactions. Are the LVZs due to the presence of over-pressurised fluids? We test this hypothesis in (4) following the numerical modelling methods of Ellis et al., [2015].

Preliminary SAHKE01 FWI Model. **See Zhao et al., Talk: S31B-06 Wed 13th 9.20 am**

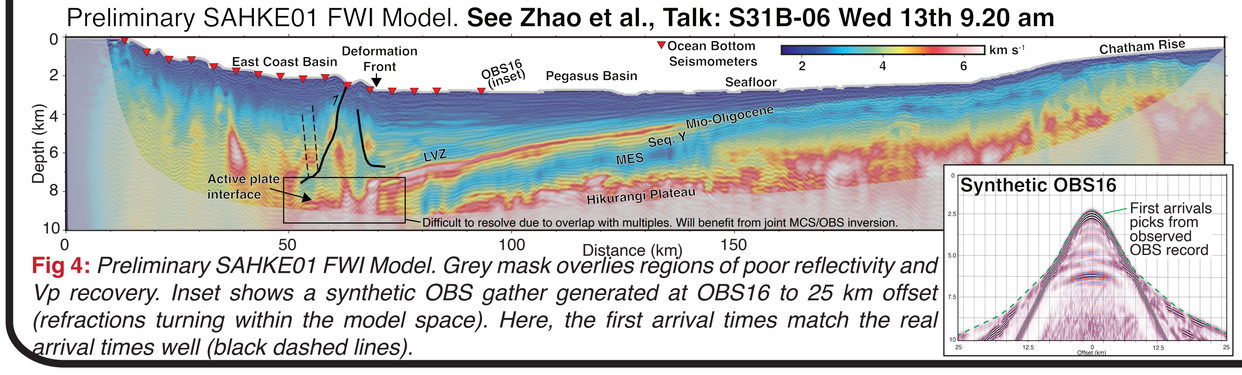

Fig 4: *Preliminary SAHKE01 FWI Model. Grey mask overlies regions of poor reflectivity and Vp recovery. Inset shows a synthetic OBS gather generated at OBS16 to 25 km offset (refractions turning within the model space). Here, the first arrival times match the real arrival times well (black dashed lines).*

4) Preliminary Numerical Modelling

To investigate which processes may be responsible for generating the observed LVZs imaged on profile 05CM38 (Fig. 3b), we performed numerical modelling using SULEC following a method similar to Ellis et al., [2015]. We estimate fluid release and effective pressure and compare the porosity field derived empirically from the V_p model with that predicted from the numerical model.

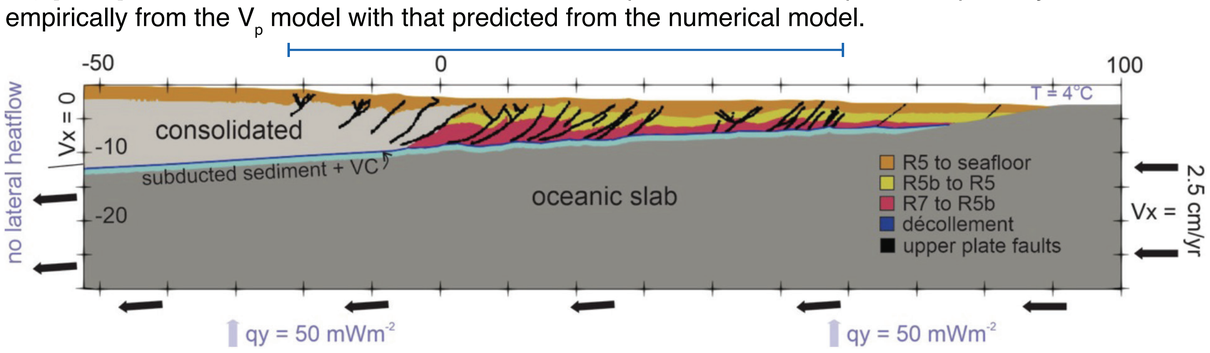

Fig 5: *Numerical model setup showing input structure and boundary conditions. The model is extrapolated outside the seismic profile bounds (blue line). qy = basal heat flow. Vx = horizontal velocity applied to the right-hand edge.*

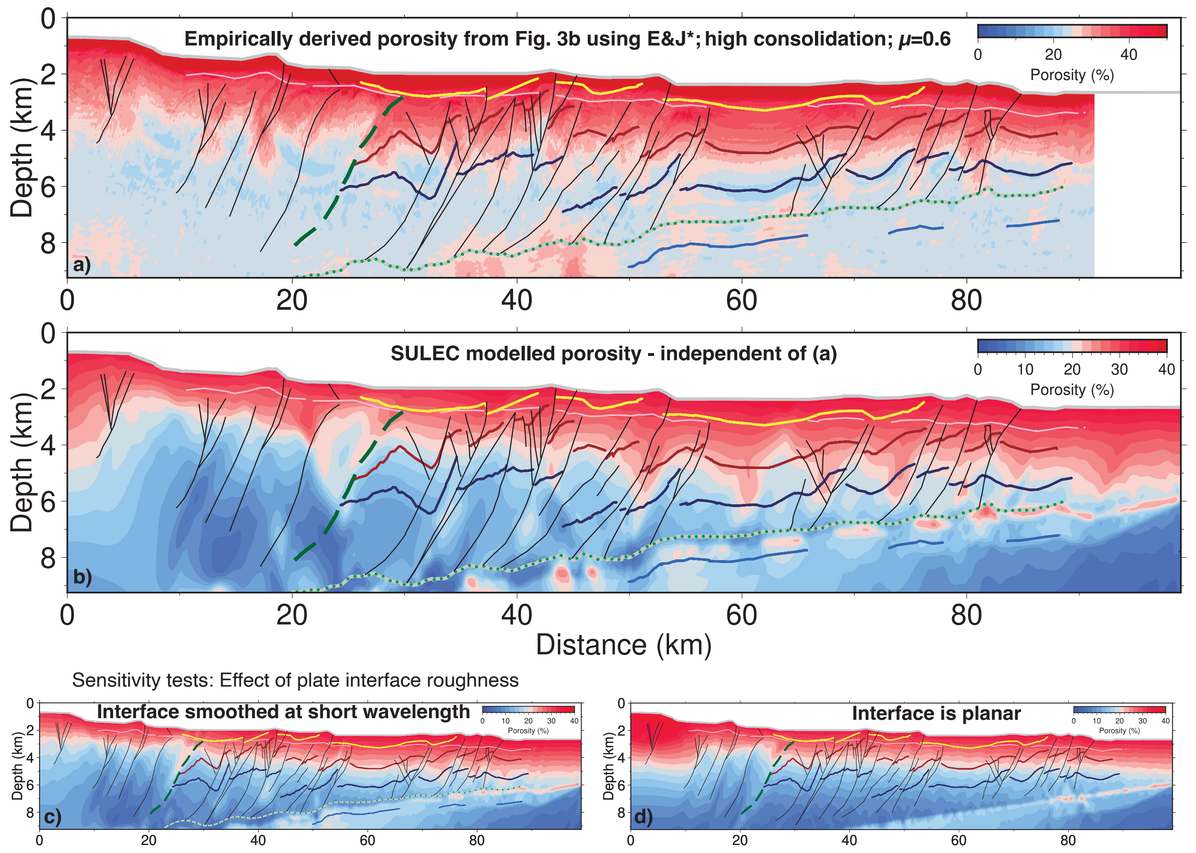

Fig 6: *a) Porosity derived using the empirical relationship of *Erickson & Jarrard [1998] for high consolidation and shale fraction=0.6 [Saffer et al., 2019]. b) Modelled porosity (note scale change - slightly reduced amplitudes relative to (a)). c) As in (b) but using a smoothed plate interface geometry. d) as in (b) but using a planar plate interface geometry. Note that the porosity variations both adjacent to thrust faults and along the plate interface are removed in (d).*

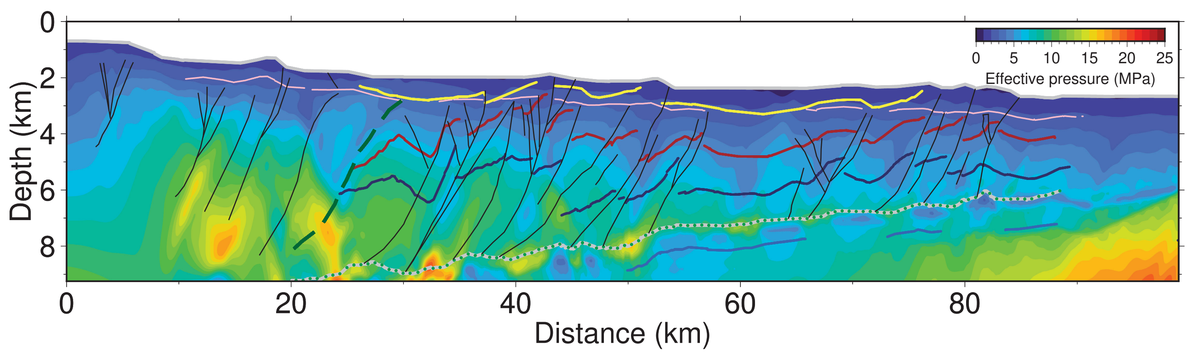

Fig 7: *Effective pressure derived from numerical modelling (mean stress-fluid pressure).*

Key finding from this model run: Plate interface roughness & tectonics appear to exert first-order control on effective pressure variations via stress variations (possibly mediated by intersection with weak upper plate faults). Fluid release via porosity loss & dehydration does occur (not shown here) but fluid pressure variations are not large enough to significantly affect effective pressure in regions where we observe LVZs.

5) Future work

See Bassett et al., Talk: T44A-04 Thur 14th 4.33 pm

- Perform joint MCS/OBS inversion on the SAHKE01 profile to extend the depth of penetration and improve Vp recovery.
- Implement multiparameter FWI including Vp/Vs and other properties (currently stable for synthetic data).
- Apply HFWI to additional legacy seismic profiles (Fig. 1) to provide a holistic view of along-strike variations in forearc & plate interface structure & physical state.
- Map fault geometries in the depth domain and compare with earthquake hypocentres.
- Incorporate FWI profiles as "ground truth" within an upcoming margin-wide 3D active-source Vp tomography model.

References

Acknowledgements:

This work is supported by public research funding from the Ministry of Business, Innovation & Employment Science Investment Fund (NZ) to GNS Science.

Z. Zhao thanks TotalEnergies E&P for supporting FWI code development. THE SEAM salt model is available at https://seg.org/SEAM/open-data

b.tozer@gns.cri.nz

- Arnulf, A. F., Biemiller, J., Lavier, L., Wallace, L. M., Bassett, D., Henrys, S., ... & Plaza Faverola, A. (2021). Physical conditions and frictional properties in the source region of a slow-slip event. Nature Geoscience, 14(5): 334-340, doi: 10.26022.
- Bangs, N.L., Morgan, J.K., Bell, R.E. et al. Slow slip along the Hikurangi margin linked to fluid-rich sediments trailing subducting seamounts. Nat. Geosci. 16, 505–512 (2023). https://doi.org/10.1038/s41561-023-01186-3
- Barnes, P. M., Lamarche, G., Bialas, J., Henrys, S., Pecher, I., Netzeband, G. L., ... & Crutchley, G. (2010). Tectonic and geological framework for gas hydrates and cold seeps on the Hikurangi subduction margin, New Zealand. Marine Geology, 272(1-4), 26-48.
- Crutchley, G. J., Klaeschen, D., Henrys, S. A., Pecher, I. A., Mountjoy, J. J., & Woelz, S. (2020). Subducted sediments, upper-plate deformation and dewatering at New Zealand's southern Hikurangi subduction margin. Earth and Planetary Science Letters, 530: 115945, doi: 10.1016.
- Ellis, S., A. Fagereng, D. Barker, S. Henrys, D. Saffer, L. Wallace, C. Williams and R. Harris, 2015, Fluid budgets along the northern Hikurangi subduction margin, New Zealand: the effect of a subducting seamount on fluid pressure, Geophysical Journal International, 202, 277-297, doi: 10.1093/gji/ggv127
- Erickson, S.N. & Jarrard, R.D., 1998. Velocity-porosity relationships for water-saturated siliciclastic sediments, J. geophys. Res.: Solid Earth (1978–2012), 103, 30 385–30 406.
- Gase, A. C., Bangs, N. L., Saffer, D. M., Han, S., Miller, P. K., Bell, R. E., ... & Barker, D. H. (2023). Subducting volcaniclastic-rich upper crust supplies fluids for shallow megathrust and slow slip. Science Advances, 9(33), eadh0150.
- Ghisetti, F. C., Barnes, P. M., Ellis, S., Plaza-Faverola, A. A., & Barker, D. H. (2016). The last 2 Myr of accretionary wedge construction in the central Hikurangi margin (North Island, New Zealand): Insights from structural modeling. Geochemistry, Geophysics, Geosystems, 17(7), 2661-2686.
- Plaza-Faverola, A., Henrys, S., Pecher, I., Wallace, L., & Klaeschen, D. (2016). Splay fault branching from the H ikurangi subduction shear zone: Implications for slow slip and fluid flow. Geochemistry, Geophysics, Geosystems, 17(12), 5009-5023.
- Saffer, D. et al. Hikurangi subduction margin coring, logging, and observatories. Site U1518. In Proc. International Ocean Discovery Program, 372B/375: College Station, TX (International Ocean Discovery Program, 2019).
- Wallace, L. M. (2020). Slow slip events in New Zealand. Annual Review of Earth and Planetary Sciences, 48, 175-203.
- Zhao, Z., Sen, M. K., Denel, B., Sun, D., & Williamson, P. (2022). A hybrid optimization framework for seismic full waveform inversion. Journal of Geophysical Research: Solid Earth, 127(8), e2022JB024483.